

OPEN ACCESS

PEFC Electrocatalysts Supported on Nb-SnO₂ for MEAs with High Activity and Durability: Part I. Application of Different Carbon Fillers

To cite this article: Y. Nakazato *et al* 2018 *J. Electrochem. Soc.* **165** F1154

View the [article online](#) for updates and enhancements.

You may also like

- [Fuel Cell Management System: PEMFC Lifetime Optimization by Model Based Approach](#)

Maxime Piffard, Ramon Naiff da Fonseca, Paolo Massioni et al.

- [Mechanical properties and microstructure of cold-rolled Scalmalloy® \(Al-4.5Mg-0.6Sc-0.3Zr alloy\) at a low reduction in thickness](#)

C Turangi, F Häslich, M Schaefer et al.

- [Doping and Defect Chemistry in LiCoO₂ By First-Principles Calculation](#)

Yukinori Koyama, Hajime Arai, Isao Tanaka et al.

Investigate your battery materials under defined force!
The new PAT-Cell-Force, especially suitable for solid-state electrolytes!



- Battery test cell for force adjustment and measurement, 0 to 1500 Newton (0-5.9 MPa at 18mm electrode diameter)
- Additional monitoring of gas pressure and temperature


www.el-cell.com +49 (0) 40 79012 737 sales@el-cell.com

EL-CELL[®]
electrochemical test equipment





PEFC Electrocatalysts Supported on Nb-SnO₂ for MEAs with High Activity and Durability: Part I. Application of Different Carbon Fillers

Y. Nakazato,¹ D. Kawachino,¹ Z. Noda,² J. Matsuda,³ S. M. Lyth,^{3,4} A. Hayashi,^{1,2,3,4,5,6,*} and K. Sasaki ^{1,2,3,4,5,6,*z}

¹Department of Hydrogen Energy Systems, Faculty of Engineering, Kyushu University, Nishi-ku, Fukuoka 819-0395, Japan

²International Research Center for Hydrogen Energy, Kyushu University, Nishi-ku, Fukuoka 819-0395, Japan

³International Institute for Carbon-Neutral Energy Research (WPI-I2CNER), Kyushu University, Nishi-ku, Fukuoka 819-0395, Japan

⁴Platform of Inter / Transdisciplinary Energy Research (Q-PIT), Kyushu University, Nishi-ku, Fukuoka 819-0395, Japan

⁵Next-Generation Fuel Cell Research Center (NEXT-FC), Kyushu University, Nishi-ku, Fukuoka 819-0395, Japan

⁶Center for Co-Evolutional Social Systems, Kyushu University, Nishi-ku, Fukuoka 819-0395, Japan

Currently, carbon black is widely used as an electrocatalyst support for polymer electrolyte fuel cells (PEFCs). However, electrochemical oxidation leads to degradation of this material. In contrast, tin oxide (SnO₂) is electrochemically stable even under strongly acidic conditions, and relatively high electronic conductivity can be achieved by doping with niobium (Nb-SnO₂), compared with other metal oxides. In this study, Nb-SnO₂ is composited with various conductive carbon fillers, including vapor-grown carbon fibers (VGCF), carbon nanotubes (CNT), and graphitized carbon black (GCB), followed by platinum nanoparticle decoration. These nanocomposite electrocatalysts are incorporated into membrane electrode assemblies (MEAs) and tested under PEFC operational conditions. The resulting fuel cells achieve high initial I-V performance up to 0.742 V at 0.2 A cm⁻² (80°C), as well as excellent cycling durability. In particular, MEAs fabricated with Pt/Nb-SnO₂/VGCF cathode electrocatalysts exhibit remarkable durability, with only a 12.1% drop in cell voltage at 0.2 A cm⁻² over 60,000 start-stop cycles, and a 42.9% drop over 400,000 load potential cycles, corresponding to the lifetime of a fuel cell vehicle (FCV). Platinum-decorated metal oxide electrocatalysts can simultaneously realize high catalytic activity and extended durability, not only in ex-situ half-cell measurements, but also in full cell conditions.

© The Author(s) 2018. Published by ECS. This is an open access article distributed under the terms of the Creative Commons Attribution Non-Commercial No Derivatives 4.0 License (CC BY-NC-ND, <http://creativecommons.org/licenses/by-nc-nd/4.0/>), which permits non-commercial reuse, distribution, and reproduction in any medium, provided the original work is not changed in any way and is properly cited. For permission for commercial reuse, please email: oa@electrochem.org. [DOI: 10.1149/2.0311814jes]



Manuscript submitted April 13, 2018; revised manuscript received October 8, 2018. Published October 23, 2018. This was Paper 1580 presented at the National Harbor, Maryland Meeting of the Society, October 1–5, 2017.

Polymer electrolyte membrane fuel cells (PEFCs) are receiving more and more attention in industry and academia as power sources.^{1,2} High performance and good durability are essential for the widespread popularization of commercial fuel cell vehicles (FCVs). The electrocatalyst layers of PEFCs have a complicated three-dimensional (3D) microstructure comprised of the catalyst, an electronic conductor, a proton conductor, and gas diffusion pathways (i.e., pores). The structure of the electrocatalyst layer critically influences the electrochemical power generation performance. Therefore, control and optimization of the microstructure and nanostructure of PEFC electrocatalyst layers are essential.

Currently, carbon black is widely used as an electrocatalyst support in PEFCs.^{1–6} However, during PEFC operation, carbon black degrades through electrochemical oxidation at the cathode, causing e.g. detachment of the Pt catalyst nanoparticles.^{2–6} Hence, improvement of the durability of PEFC catalyst supports has been attempted by using more stable alternative cathode materials such as graphene,^{7,8} CNTs,^{9,10} mesoporous carbon,^{11,12} and nitrogen-doped carbon.¹³ However, the only way to completely avoid carbon corrosion is to develop carbon-free electrocatalyst supports - metal oxides have emerged as promising materials for this.^{14–25} Examples of metal oxide supports that are stable under cathodic conditions¹⁹ include titanium oxide^{14–16} and tungsten oxide.¹⁷

Amongst the various different types of metal oxide, SnO₂ has relatively high electronic conductivity, and good stability under the strongly-acidic conditions in a PEFC.^{18–20} For this reason, SnO₂ is one of the most promising carbon-free support materials, and many studies have been performed exploring the use of this material in PEFCs.^{21–35}

Our group first proposed the use of SnO₂ as an electrocatalyst support as early as 2004.²¹

In order to examine the suitability of SnO₂ as a durable catalyst support material in PEFCs, many groups have applied potential cycling to their electrocatalyst systems. In particular, start-stop potential cycling protocols have been used up to high potential, to simulate the start-stop cycles in a real FCV, which cause carbon corrosion. Masao et al.²² and Takasaki et al.²³ reported that SnO₂-supported Pt electrocatalysts maintained their electrochemical surface area (ECSA) even after 60,000 start-stop cycles, which was verified through half-cell tests using rotating disk electrode (RDE) voltammetry. Kanda et al. reported that SnO₂-supported electrocatalysts maintained high cell voltage even after 60,000 start-stop cycles in a membrane electrode assembly (MEA).²⁴ In other groups, for example, Kakinuma et al. and Mohanta et al. reported that Sb-doped SnO₂ could maintain its ECSA after potential cycling.^{31,32}

However, SnO₂-based materials have lower electronic conductivity compared to carbon black. Therefore, whilst the durability of SnO₂ under potential cycling is excellent, in early works, it was difficult to achieve sufficient electrochemical performance. To be used in future FCVs, PEFCs have to exhibit cell voltage higher than e.g. 0.8 V at 0.2 A cm⁻² for better efficiency and downsizing of PEFC system size. One way to overcome the issue of low conductivity is to reintroduce carbon as a conductive filler in electrocatalyst layers, instead of as the electrocatalyst support. SnO₂-based electrocatalyst supports dispersed on carbon materials such as CNTs, have shown high electrocatalytic activity and stability in half-cell RDE measurements.^{33–35} However, there are still only a few reports of MEA evaluation using such electrocatalysts.³⁶ Whilst carbon nanotube fillers have been shown to act as conductive pathway to improve MEA performance, the performance of different types of conductive carbon filler has not yet been investigated systematically, to the best of our knowledge.

*Electrochemical Society Member.

^zE-mail: sasaki@mech.kyushu-u.ac.jp

The type of carbon used as a conductive filler for SnO₂-based electrocatalyst supports should be carefully considered. The surface area and porosity are expected to strongly influence the MEA performance. In addition, the degree of graphitization is important – highly graphitic carbons are kinetically more stable against electrochemical oxidation.^{37–40} The degree of graphitization is also important in making sure that platinum decoration occurs mainly on the SnO₂ and not on the carbon – the binding energy between Pt and graphitized carbon is much lower than that between Pt and SnO₂, leading to selective deposition on the metal oxide.^{39–41}

Here, the aim of this study is to develop MEAs achieving both high I-V performance and high potential cycle durability in MEAs, using platinum-decorated niobium-doped tin oxide (Pt/Nb-SnO₂) with various conductive carbon fillers. The representative carbon nanomaterials selected for this study are VGCF, CNT, and GCB. These different materials are used to vary the electrocatalyst layer microstructure and conductivity, and we investigate the resulting changes in electrocatalyst activity, MEA cell performance, and durability.

Experimental

Characterization of carbon fillers.—Three types of conductive fillers were used in this study: VGCFs (VGCF-H, diameter: 150 nm diameter, Showa Denko, Japan), CNTs (MW-1 dispersed in sodium dodecylbenzene sulfonate (SDBS) surfactant, 15 nm diameter, Meijo Nano Carbon Co., Ltd, Japan), and GCBs (FCX200, Cabot, US). The Brunauer-Emmett-Teller (BET) surface area of these carbon materials was characterized by nitrogen adsorption measurements (BELSORP-mini, MicrotracBEL Corp., Japan).

In order to evaluate the through-plane electrical conductivity of the electrocatalyst layers, the carbon materials were mixed with 5% Nafion solution as a binder, and spray-printed onto a Pt foil substrate (10 × 10 × 0.3 mm) with a carbon loading of 3.8 mg cm⁻², an electrode area of 0.5 cm², and a porous carbon layer thickness of ca. 100 μm. The relative density was ca. 20%, and the Nafion content in the resulting layers was 0.2 mg cm⁻², i.e., 5 wt%. A layer of Pt (10 nm) was sputtered onto the carbon layer to minimize contact resistance, and an insulating film was attached on the exposed areas of the Pt substrate to prevent short circuiting. A second Pt foil electrode was then sandwiched on the top surface. Each platinum foil electrode was attached to a Pt mesh spot-welded with two Pt wires acting as the current and voltage probes. The through-plane conductivity was then measured using 4-point probe measurements with an AC impedance analyzer (1255B, Solartron). Vulcan-XC72 (Cabot, US) was also tested for comparison.

Preparation of electrocatalysts.—Nb-SnO₂ support materials were prepared by the ammonia co-precipitation method, or the microwave-assisted homogeneous precipitation method, according to previously published procedures.³⁴ SnO₂ was doped with Nb⁵⁺ as an electron donor to improve the electronic conductivity,²³ and the molar ratio of Nb in Nb-SnO₂ was selected to be 2 mol%. Electrocatalyst preparation procedures are summarized in Figure 1. The SnO₂ deposition method was selected by considering the surface area of the conductive fillers. Preliminary results revealed that typical grain size of SnO₂ prepared via ammonia co-precipitation was several tens of nanometers, compared with a few nanometers for the microwave-assisted homogeneous precipitation method. Thus, the ammonia co-precipitation method was suitable for fillers with relatively small surface area, whilst the microwave-assisted homogeneous precipitation method was suitable for fillers with larger surface area, with respect to the homogeneity of SnO₂ particle distribution. Consequently, the selected method depended on the nature of the carbon filler material.

Ammonia Co-precipitation method.—An ultrasonic homogenizer (UH-600, SMT Co., Ltd, Japan) was used for dispersing the conductive fillers in 500 ml of ethanol for 30 minutes. SnCl₂ · 2H₂O (Kishida Chemical Co. Ltd., Japan) and NbCl₅ (Kishida Chemical Co. Ltd.,

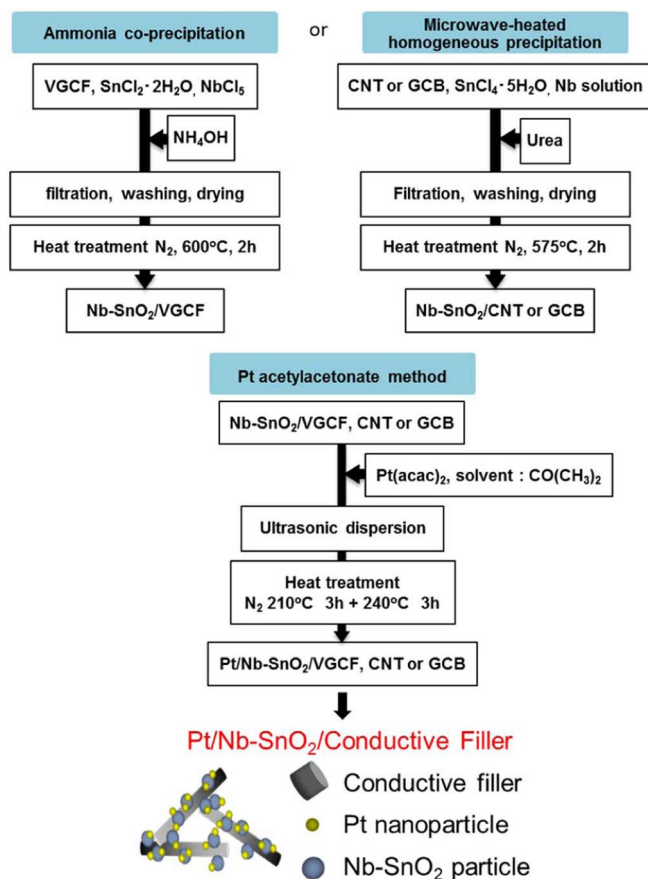


Figure 1. Preparation protocols of Pt/Nb-SnO₂/carbon electrocatalysts.

Japan) dissolved in ethanol were added into the dispersion, which was then homogenized using a high-speed stirrer at 1000 rpm. A mixture of 28% ammonia solution (24 ml) and ultra-pure water (96 ml) was then added into the dispersion dropwise, at room temperature, then homogenized for 1 h. The dispersion was filtered, and re-dispersed in ultra-pure water twice to purify the product, then dried at 100°C for 10 h. Finally, the dried product was heat-treated at 600°C under flowing N₂ for 2 h. The loading of Nb-SnO₂ on the carbon filler was 50 wt%, i.e., the weight ratio of Nb-SnO₂ and the carbon filler was 50:50.

Microwave-assisted homogeneous precipitation method.—The same ultrasonic homogenizer was used for dispersing the conductive fillers in 150 ml of ultra-pure water, for 30 minutes. SnCl₄ · 5H₂O (Kishida Chemical Co Ltd., Japan), urea (Kishida Chemical Co. Ltd, Japan), and Nb standard solution (AccuStandard, ICP-MS-38W-1) were added to the dispersion. The dispersion was stirred at 2000 rpm for 30 minutes at room temperature, then heated at 90°C for 25 minutes using a microwave irradiation device (μ reactor EX, Shikoku Instrumentation, Japan). The dispersion was filtered, and re-dispersed in ultra-pure water twice to purify the product, then dried at 100°C for 10 h. Finally, the dried product was heat-treated at 575°C under flowing N₂ for 2 h. The loading of Nb-SnO₂ and the carbon filler was 70:30, i.e., the weight ratio of Nb-SnO₂ and the carbon filler was 70:30.

Pt-decoration was performed via the platinum (II) acetylacetonate method. This method uses platinum (II) acetylacetonate as a precursor, followed by thermal reduction of Pt(II) to Pt(0). This method results in a high degree of control and reproducibility.⁴² Here, the Pt loading was set to be ~20 wt%. In a 300 ml flask, the Nb-SnO₂/carbon and Pt(II) acetylacetonate (Pt(acac)₂, Sigma-Aldrich Co., LLC) were dispersed/dissolved in 50 ml of acetone (Kanto Kagaku, Japan) via ultrasonication. Following this, the solvent was evaporated in vacuum,

Table I. Preparation conditions of MEAs.

	Anode	Cathode
Electrocatalyst	Pt/C (TEC10E50E)	Pt/Nb-SnO ₂ /VGCF Pt/Nb-SnO ₂ /CNT Pt/Nb-SnO ₂ /GCB Pt/C (TEC10E50E)
Electrolyte membrane	Nafion 212	
Gas diffusion layer	Carbon paper	MPL carbon paper (25BC)
Electrode area/cm ²	1.0	1.0
Pt loading/mg cm ⁻²	0.3	0.3
Nafion ratio/wt%	28	3, 8, 11, 13, 15, 18, 23, 28

and the remaining solid was heat-treated under flowing N₂ at 210°C for 3 h, then at 240°C for 3 h, with a heating rate of 1°C min⁻¹.

Characterization of electrocatalysts.—The resulting electrocatalysts were observed using a field-emission scanning electron microscope (FE-SEM, S-5200, Hitachi High-Technologies) and a transmission electron microscope (TEM, JEM-ARM200F, JEOL). The Pt loading was quantified by using inductively coupled plasma atomic emission spectroscopy (ICP-AES, Shimadzu, ICPE-9000). Electrochemical characterization was performed on an automatic polarization system (HZ-5000, Hokuto Denko Corp., Japan), using protocols proposed by the Fuel Cell Commercialization Conference of Japan (FCCJ).⁴³ An Ag/AgCl electrode in saturated KCl was used as the reference electrode, and a Pt wire was used as the counter electrode. The electrolyte solution was 0.1 M HClO₄, at 25°C. The electrocatalyst dispersion was blended with Nafion ionomer solution, then deposited carefully onto the Au disk of the working electrode (area: 0.196 cm²). The electrochemical surface area (ECSA) was determined from the hydrogen desorption charge (Q_H) in cyclic voltammograms scanned between 0.05 and 1.2 V_{RHE} at 50 mV s⁻¹ in N₂-saturated HClO₄. The mass activity (MA) at 0.9 V_{RHE} was derived using the kinetic current obtained from Koutecky-Levich plots plotted from linear sweep voltammogram (LSV), using the rotating disk electrode (RDE) in O₂-saturated HClO₄. The disk rotation speed was varied from 2500, to 1600, 900, and 400 rpm. The potential range was 0.2 to 1.2 V_{RHE}, and the scanning rate was 10 mV s⁻¹.

Preparation of MEAs.—The MEA preparation conditions are compiled in Table I. Electrocatalyst paste was prepared by dispersing the Pt/Nb-SnO₂/carbon powder (or Pt/C, 46.4 wt% TEC10E50E, Tanaka Kikinzoku Kogyo Corp., Japan), 99.5% ethanol, ultra-pure water, and 5% Nafion solution, using the ultrasonic homogenizer. This electrocatalyst paste was printed onto the electrolyte membrane (Nafion 212) using a spray printing system (C-3 J, Nordson). The electrode area was 1.0 cm² (1 cm × 1 cm). Electrocatalysts containing the three different types of conductive carbon filler were applied to the cathode, and the Pt loading was set to be 0.3 mg_{Pt} cm⁻² in each case. For the anode, the standard 46.4% Pt/C was used, and the Pt loading was also set to be 0.3 mg_{Pt} cm⁻². After spray printing, the resulting MEA was dried overnight, then hot-pressed at 132°C at 0.3 kN, for 180 seconds. Finally, both electrodes were sandwiched between gas diffusion layers (GDL), comprising of Teflon-coated carbon paper with (25BC, SGL Carbon) and without (EC-TP1-060T, Electrochem) a microporous layer (MPL), for the cathode and the anode, respectively.

Characterization of MEAs.—I-V characteristics of MEAs were evaluated at 80°C and 100% relative humidity (RH). The cell temperature and the gas humidification temperature were both 80°C, and the gas utilization of H₂ and air was set to be 2% for both the cathode and the anode. A cell holder developed in a New Energy and Industrial Technology Development Organization (NEDO) project^{44,45} was used for MEA evaluations. Before actual I-V measurements, MEAs were pre-treated at 0.5 V for 5 h. For evaluating various overvolt-

Table II. Electrical conductivity of various carbon filler materials at 25 and 80°C.

Carbon materials	Thickness/μm	Temperature/°C	Specific electrical conductivity/S cm ⁻¹
VGCF	108	25	7.2
		80	8.5
CNT	117	25	12.5
		80	13.2
GCB	73	25	4.7
		80	5.4
Vulcan-XC72	87	25	5.2
		80	6.1

age contributions, the ohmic cell resistance was measured by the AC impedance analyzer (1255B, Solatron), and the IR losses were separated, by subtracting the ohmic contribution (IR losses) from the recorded cell voltage. The IR-free voltage losses were then separated into activation overvoltage and concentration overvoltage. A Tafel plot was created according to NEDO protocols,^{44,45} with current density plotted on the logarithmic x-axis, and the IR-free cell voltage plotted on the y-axis. In the low current density region, 3 to 4 values were fitted with a linear regression. The difference between the theoretical electromotive force (1.17 V at 80°C for a H₂/air cell at ambient pressure) and the voltage of the linear regression line was taken as the activation overvoltage at the current density of interest. The deviation of the IR-free voltage from the voltage at the linear regression line in the Tafel plot was taken as the concentration overvoltage.⁴⁵ As well as electrochemical characterization of MEAs, the microstructure of the cathode layers within the MEAs was evaluated using a focused ion beam coupled with scanning electron microscopy (FIB-SEM, Helios NanoLab 600i, FEI).

To evaluate the durability of MEAs, accelerated degradation tests were performed. A protocol simulating the start-stop cycles of an FCV was used, as recommended by the FCCJ⁴³ and NEDO.⁴⁵ According to this protocol, a triangular potential waveform between 1.0 and 1.5 V was used, with 2 seconds per cycle. A protocol simulating FCV load cycles, also recommended by the FCCJ⁴³ and NEDO,⁴⁵ was also used, where a rectangular potential waveform between 0.6 and 1.0 V was used, with 6 seconds per cycle.

Results and Discussion

Characterization of carbon materials.—The BET surface areas of VGCF, CNT, and GCB were 10.8, 45.9, and 34.5 m² g⁻¹, respectively. The smaller surface area of VGCF compared with CNT and GCB means that the ammonia co-precipitation method is more suitable for VGCFs whilst the microwave-assisted homogeneous precipitation method more suitable for CNTs and GCBs.

The electrical conductivity of VGCF, CNT, GCB, and Vulcan-XC72 carbon layers prepared by spray printing with Nafion binder is compiled in Table II. A weak temperature dependency is observed. The ionic conductivity of Nafion ionomer is much lower than the electronic conductivity of carbon, with strong temperature dependency,^{46,47} so the measured conductivity can be assumed to originate from the carbon materials, rather than Nafion binder. These results indicate that the selected carbon nanomaterials exhibit comparable or higher electrical conductivity compared with the typical carbon materials used in PEFC electrocatalysts (i.e. Vulcan-XC72).

Preparation and characterization of electrocatalysts.—Representative FE-SEM images of the different electrocatalyst materials prepared for this study are shown in Figure 2. These include Pt/Nb-SnO₂/VGCF, Pt/Nb-SnO₂/CNT, Pt/Nb-SnO₂/GCB, and conventional Pt/C. Figure 2a shows the Pt/Nb-SnO₂/VGCF electrocatalyst. The VGCFs can clearly be seen crossing the image, with a diameter of around 150 nm. Coating these fibers are nanoparticles of Nb-SnO₂, uniformly dispersed on the surface of the VGCFs.

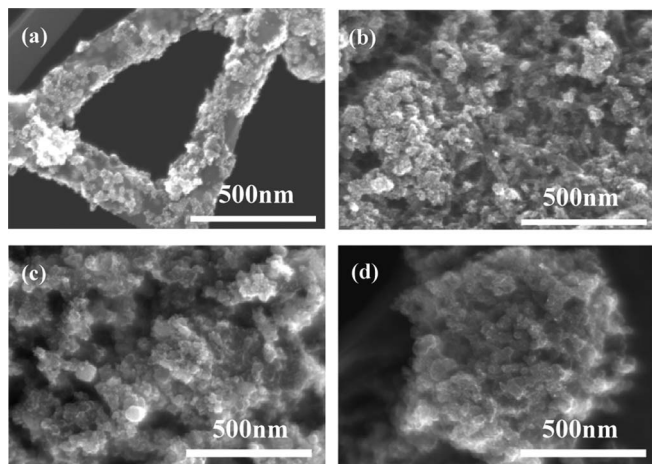


Figure 2. FE-SEM images of (a) Pt/Nb-SnO₂/VGCF, (b) Pt/Nb-SnO₂/CNT, (c) Pt/Nb-SnO₂/GCB, and (d) conventional Pt/C electrocatalysts.

Figure 2b shows the Pt/Nb-SnO₂/CNT electrocatalyst. Here, the individual CNTs can just be made out, with a diameter of around 15 nm. However, in this case, the Nb-SnO₂ nanoparticles do not appear to be clearly decorated on the carbon surface, and they form larger aggregates. This may be due to clustering of the CNTs by van der Waals forces,^{48–50} despite the use of SDBS surfactant. Another contributing factor may be that the size of the Nb-SnO₂ nanoparticles is quite large compared to the CNT diameter, making uniform decoration more difficult. Figure 2c shows the Pt/Nb-SnO₂/GCB electrocatalyst. In this case it is more difficult to distinguish between the Nb-SnO₂ and the carbon, as the nanoparticle size and shape are similar. However, it appears that the Nb-SnO₂ particles are fairly uniformly dispersed, but do not coat the entire surface of the GCB. Figure 2d shows the conventional Pt/C electrocatalyst. Here a large aggregation of carbon black can be observed, and the platinum nanoparticles are observed as bright spots on the surface.

The electrocatalytic activity (i.e. ECSA and mass activity) of the catalysts, measured by half-cell tests, is shown in Figure 3. The Pt/Nb-SnO₂/CNT electrocatalyst exhibited the largest ECSA and the highest mass activity among the prepared electrocatalysts (although still lower than for Pt/C). Pt/Nb-SnO₂/VGCF has the lowest ECSA, whilst Pt/Nb-SnO₂/GCB has the lowest mass activity. The ECSA of the different catalysts with the Nb-SnO₂ support varies in good agreement with the BET surface area (i.e. 18.4, 102.5, and 34.9 m² g⁻¹ for Pt/Nb-SnO₂/VGCF, Pt/Nb-SnO₂/CNT, and Pt/Nb-SnO₂/GCB, respectively). On the other hand, the mass activity does not follow the BET surface area, suggesting that a different mechanism other than surface area contributes to the performance. This could be attributed to the different ways Nb-SnO₂ is dispersed on the carbon filler, depending on the microstructure, the conductivity, or to differences in the Pt nanoparticle size (as discussed later). Therefore, it seems that fibrous conductive fillers (such as VGCF and CNT) are more suited to achieve high mass activity.

I-V Characteristics of MEAs.—MEAs were prepared from the Pt/Nb-SnO₂/VGCF, Pt/Nb-SnO₂/CNT, and Pt/Nb-SnO₂/GCB electrocatalysts. The Nafion ratio (wt%) in the cathode electrocatalyst layer was varied, to optimize the I-V performance as shown in Figure 4. The I-V characteristics of the MEAs with different Nafion ratios for the standard Pt/C measured under the identical conditions have already been published by Okumura et al.⁵¹ For the Pt/Nb-SnO₂/VGCF-based MEA, the highest I-V performance was obtained with a Nafion ratio of 23 wt%. However, both Pt/Nb-SnO₂/CNT-based and Pt/Nb-SnO₂/GCB-based MEAs exhibited the highest I-V performance when the Nafion ratio was just 13 wt%. When too much Nafion ionomer was added, the I-V performance decreased rapidly in all cases, especially in the high current density region. This is proba-

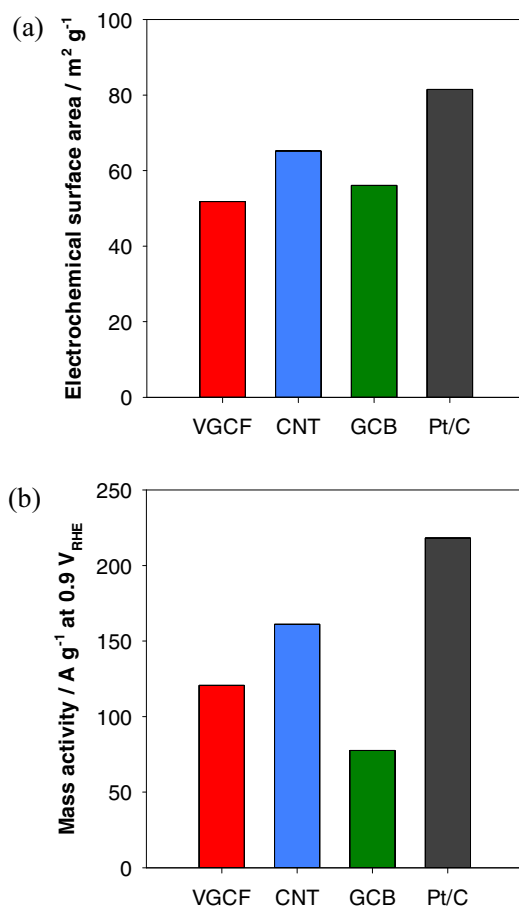


Figure 3. Initial electrocatalytic activity of the Pt/Nb-SnO₂/VGCF, Pt/Nb-SnO₂/CNT, Pt/Nb-SnO₂/GCB, and Pt/C electrocatalysts: (a) electrochemical surface area (ECSA) and (b) mass activity (measured at 0.9 V_{RHE}).

bly due to increased concentration overvoltage, as discussed in more detail below.

In order to gain more insight into the factors affecting the cell voltage, the total overvoltage was separated into 3 different contributions: the activation overvoltage, IR losses, and the concentration overvoltage, as shown in Figure 5. The activation overvoltage and IR losses at 0.2 A cm⁻² are plotted, whilst the concentration overvoltage at 1.0 A cm⁻² is plotted for clarity. There is almost no change in the IR loss (i.e. the ohmic resistance) as the Nafion content changes, in all cases. This suggests that the conductivity of the electrocatalyst layer is not significantly affected by the Nafion ratio.

On the other hand, the concentration overvoltage varies more significantly with Nafion content. For Pt/Nb-SnO₂/VGCF, the MEA with 23 wt% Nafion exhibits the lowest concentration overvoltage, for Pt/Nb-SnO₂/CNT, the MEA with 8 wt% Nafion exhibits the lowest concentration overvoltage, and for Pt/Nb-SnO₂/GCB, the MEA with 18 wt% Nafion exhibits the lowest concentration overvoltage. In all cases the concentration overvoltage then clearly increases as the Nafion content increases further. A similar trend is seen in the case of the activation overvoltages. Efficient fuel cell reactions require the presence of well-optimized three-phase boundaries. The dependency of activation overvoltage on the Nafion content is most likely related to insufficient contact between ionomer and the Pt catalyst at low Nafion content, and the ionomer is completely coating the Pt nanoparticles at high Nafion content. In the case of concentration overvoltage, the ionomer is expected to block gas diffusion pathways at higher Nafion content.^{51,52} The difference in overvoltages depending on the different carbon filler used is a result of the very different microstructure of the cathode layer in each case. In particular, the Pt/Nb-SnO₂/CNT sample

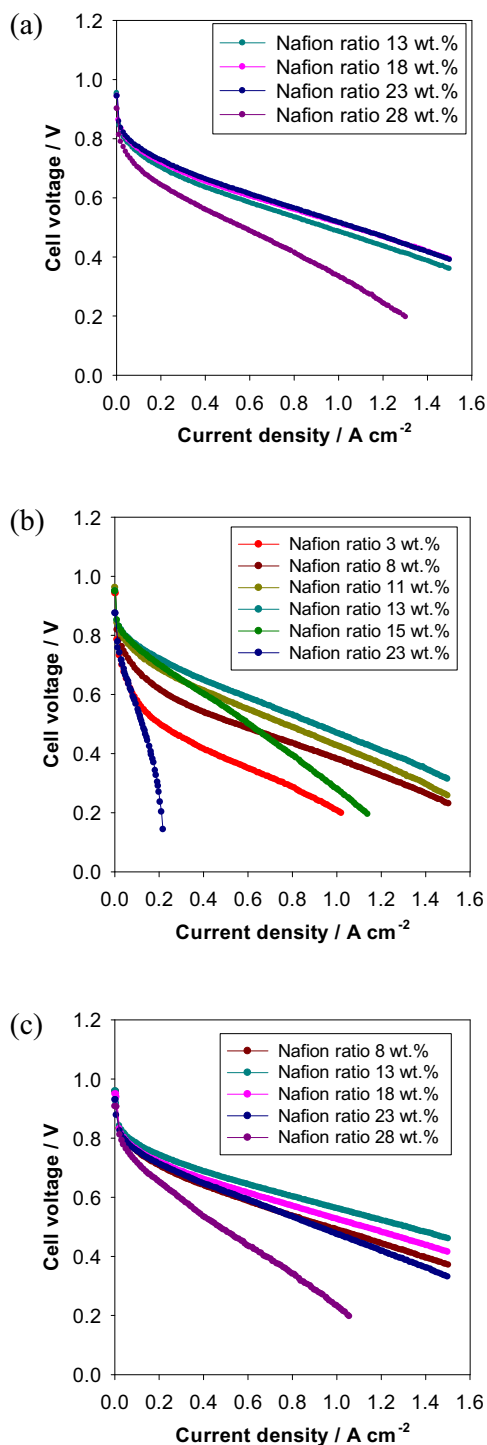


Figure 4. Initial I-V characteristics of MEAs made with (a) Pt/Nb-SnO₂/VGCF, (b) Pt/Nb-SnO₂/CNT, and (c) Pt/Nb-SnO₂/GCB cathodes. In each case the Nafion ratio was varied, and the anode was Pt/C. Measurements were performed at 80°C and RH 100%.

shows a much larger variation in the I-V characteristics with changing Nafion content.

The microstructure of the cathode layers of MEAs prepared with the different electrocatalysts was observed by FIB-SEM, for the best-performing MEA Nafion ratio in each case. Cross-sectional SEM micrographs of each cathode layer are shown in Figure 6. In the Pt/Nb-SnO₂/VGCF cathode layer, large micron-scale pores co-exist with many smaller pores, with a large pore-size distribution.

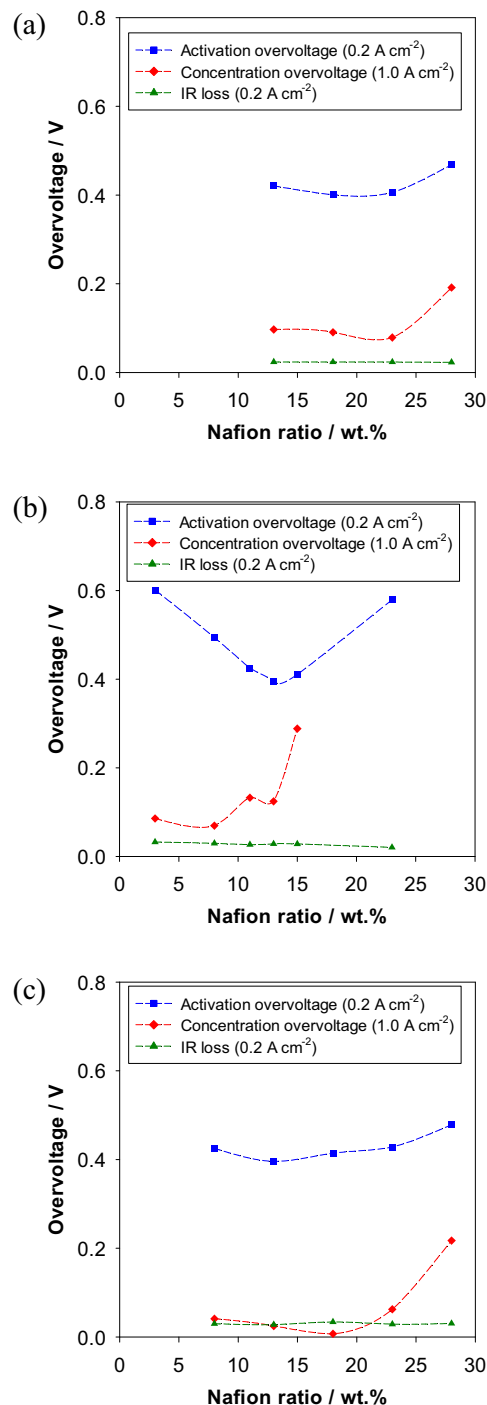


Figure 5. Separated overvoltages of MEAs made with (a) Pt/Nb-SnO₂/VGCF, (b) Pt/Nb-SnO₂/CNT, and (c) Pt/Nb-SnO₂/GCB cathodes, and their dependence on the Nafion ratio in the cathode catalyst layer. In each case the anode was Pt/C. Measurements were performed at 80°C and RH 100%.

In contrast, the Pt/Nb-SnO₂/CNT cathode layer is relatively dense and includes much smaller pores. In the Pt/Nb-SnO₂/GCB cathode layer, the pore size distribution is similar to that observed in the conventional Pt/C reference cathode layer,⁵¹ with slightly larger pores than the case of Pt/Nb-SnO₂/CNT. These SEM images can be linked with the trends observed in the overvoltage data. The large pores in Pt/Nb-SnO₂/VGCF act as efficient gas diffusion and water exhaust pathways, thus a higher Nafion ratio can be accommodated in the electrocatalyst layer without increasing the concentration overvolt-

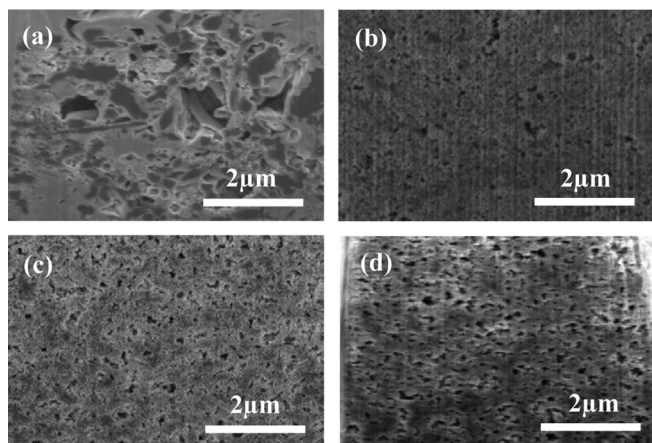


Figure 6. FIB-SEM cross-sectional images of MEA cathodes with (a) Pt/Nb-SnO₂/VGCF (23 wt% Nafion), (b) Pt/Nb-SnO₂/CNT (13 wt% Nafion), (c) Pt/Nb-SnO₂/GCB (13 wt% Nafion), and (d) Pt/C (28 wt% Nafion).

age. The smaller pores in Pt/Nb-SnO₂/CNT and Pt/Nb-SnO₂/GCB are more quickly filled by excess Nafion and water generated at the cathode, leading to an increase in concentration overvoltage at higher Nafion content, as observed.

Start-stop cycle durability of MEAs.—The durability of MEAs incorporating the electrocatalysts was evaluated by applying potential protocols simulating the start-stop cycles of an FCV. The results are shown in Figure 7. Figure 7a shows how the cell voltage at 0.2 A cm⁻² changes over 60,000 potential cycles. Whilst the initial cell voltage of the MEA with the Pt/C catalyst is high, this rapidly falls in the first few thousand cycles, and then gradually decreases up to 60,000 cycles. In contrast, none of the Nb-SnO₂-based electrocatalysts show a rapid voltage drop in the first few thousand cycles. The Pt/Nb-SnO₂/VGCF MEA has the highest cell voltage retention, at 87.9% (i.e., 12.1% drop) after 60,000 start-stop cycles. The Pt/Nb-SnO₂/CNT MEA maintained its initial cell voltage even after 10,000 start-stop cycles, but only 60.6% of the initial cell voltage is retained after 60,000 start-stop cycles. The Pt/Nb-SnO₂/GCB MEA loses 12.0% of its initial cell voltage in the first 5,000 start-stop cycles, but eventually 80.3% of the initial cell voltage is retained after 60,000 start-stop cycles. The high cell voltage retention of these Pt/Nb-SnO₂/carbon MEAs under start-stop cycling conditions is attributed to the stability of the Nb-SnO₂ support, which cannot be further oxidized under such high potential conditions.

Figure 7b shows the change in ECSA of these MEAs over 60,000 start-stop potential cycles. The Pt/C MEA has high initial ECSA, but this rapidly drops to around 40 m² g⁻¹ over the first few thousand cycles, after which it is reasonably stable. In contrast, all of the Nb-SnO₂-based MEAs have an initial ECSA of between 30 and 40 m² g⁻¹, but this is retained over the whole 60,000 cycles. This stability is attributed to the fact that Pt nanoparticles deco-

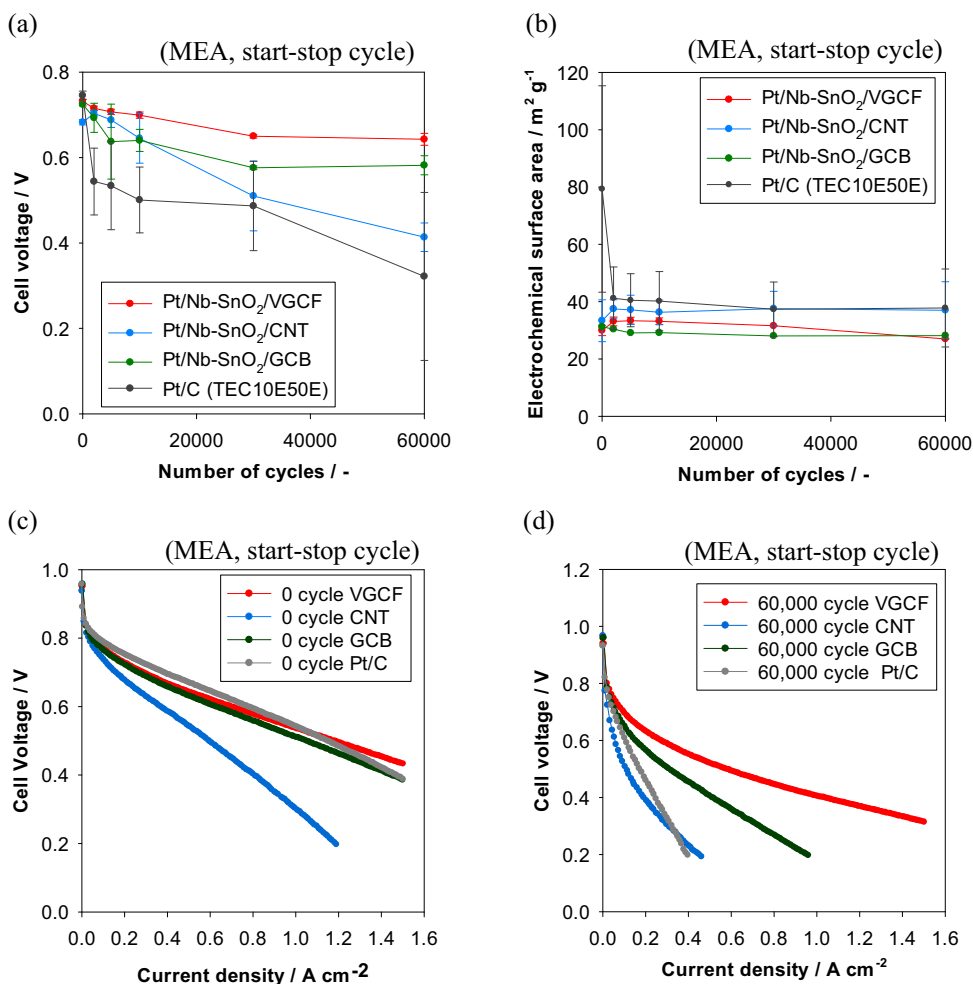


Figure 7. (a) Cell voltage at 0.2 A cm⁻², (b) ECSA, and I-V characteristics of MEAs made with Pt/Nb-SnO₂/VGCF, Pt/Nb-SnO₂/CNT, Pt/Nb-SnO₂/GCB, and Pt/C, (c) before, and (d) after 60,000 start-stop potential cycles.

rated on Nb-SnO₂ are more stable against detachment and/or agglomeration, due to increased binding energy between Pt and SnO₂, compared to Pt and carbon,⁴¹ as well as selective decoration of Pt nanoparticles directly on the Nb-SnO₂ rather than the carbon fillers. Direct contact between Pt catalysts and the carbon fillers would catalyze carbon oxidation, however this is prevented by the presence of SnO₂.

Figure 7c and 7d shows the I-V characteristics before and after the 60,000 start-stop cycles, respectively. Whilst it must be expected that these novel electrocatalysts will have slightly lower activity than Pt/C, it is clear that the initial performance is comparable. It is also evident that the performance of Pt/Nb-SnO₂/VGCF (and to a lesser extent Pt/Nb-SnO₂/GCB), maintain their electrochemical performance much more effectively than the conventional Pt/C electrocatalyst.

Representative TEM images of each electrocatalyst before and after MEA start-stop cycle durability tests are shown in Figure 8. The average Pt particle diameter obtained from the TEM images is shown in Figure 9, with standard deviation. The average Pt particle diameter increased after start-stop potential cycling in all cases, but the grain growth kinetics were clearly different for each different electrocatalyst. The Pt particle diameter in Pt/Nb-SnO₂/VGCF increased by 22.9%, in Pt/Nb-SnO₂/CNT by 4.5%, and in Pt/Nb-SnO₂/GCB by 27.5%, respectively. In contrast, the Pt particle size increased by a much larger amount (72.1%) for Pt/C. This is further evidence of the increased stability of Pt on Nb-SnO₂ supports.

The microstructure and thickness of the cathode layer of the MEAs were also evaluated before and after the start-stop cycles. Carbon mass retention with respect to Pt mass was derived from quantitative elemental analysis using TEM-EDS. The thickness and carbon mass retention of each cathode layer are summarized in Figure 10. Cross-sectional SEM micrographs of each cathode layer before and after cycling are also shown in Figure 11. For the MEA using the conventional Pt/C, the cathode layer decreased to just 49.4% of the initial thickness, and the carbon mass decreased to 62.7% of the initial mass after 60,000 start-stop cycles. For Pt/Nb-SnO₂/CNT, the thickness decreased to 73.1% of the initial value, and carbon mass retention was 52.3%. For Pt/Nb-SnO₂/GCB, the thickness decreased to 90.4% of the initial value, and carbon mass decreased to 56.1% of the initial mass. However, in the case of Pt/Nb-SnO₂/VGCF there was no clear change in cathode layer thickness, carbon mass ratio, and microstructure. In the case of Pt/C, it is clear that carbon oxidation leads to a significant thinning of the electrocatalyst layers. However, in the Nb-SnO₂-based electrocatalysts, this thinning is not as pronounced, and in the case of VGCF is negligible. This is direct evidence that the presence of SnO₂ prevents carbon oxidation during PEFC operation.

These differences in the degradation of these catalysts during start-stop operation are likely caused by a combination of differences in surface area, the uniformity of the Nb-SnO₂ support, and the resulting distribution of Pt nanoparticles. In the case of Pt/C, platinum is in direct contact with the carbon, leading to severe carbon corrosion during operation. In the case of VGCF, the Nb-SnO₂ is very well distributed on the surface of the carbon, and the Pt nanoparticles are mainly attached to the Nb-SnO₂. This is expected to prevent carbon corrosion. In the cases of Pt/Nb-SnO₂/CNT and Pt/Nb-SnO₂/GCB, the Nb-SnO₂ was not as uniformly distributed on the carbon surface (Figure 2). In this case, some of the Pt nanoparticles would have been attached directly to the carbon, leading to some carbon corrosion, but to a lesser extent than in Pt/C.

Load cycle durability of MEAs.—For MEAs incorporating selected electrocatalysts, i.e., Pt/Nb-SnO₂/VGCF and conventional Pt/C, load potential durability tests were performed up to 400,000 cycles, as shown in Figure 12. Figure 12a shows that, for both MEAs the cell voltage at 0.2 A cm⁻² gradually decreases as the number of load cycles increases. For Pt/Nb-SnO₂/VGCF, the cell voltage decreases more sharply up to ~50,000 load cycles, and after that, gradually decreases compared to the MEA incorporating conventional Pt/C. The cell voltage retention after 400,000 load cycles is 57.1% (i.e., a drop of 42.9%) for Pt/Nb-SnO₂/VGCF, comparable to the value of 57.3% for

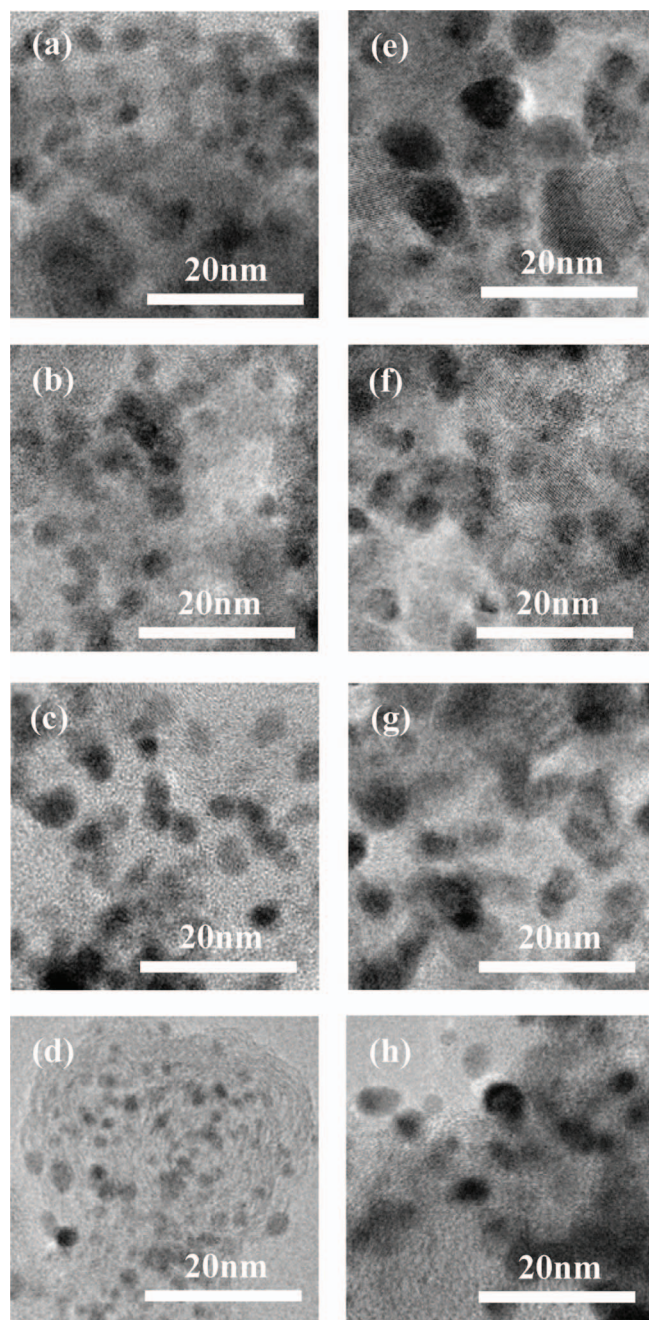


Figure 8. TEM images of the electrocatalysts (a-d) before and (e-h) after 60,000 start-stop potential cycles: (a,e) Pt/Nb-SnO₂/VGCF (b,f) Pt/Nb-SnO₂/CNT (c,g) Pt/Nb-SnO₂/GCB, and (d,h) Pt/C.

Pt/C. The initial ECSA of the Pt/Nb-SnO₂/VGCF MEA was approximately half that of Pt/C. However, after losing ~20% of the initial ECSA up to 50,000 cycles, there is negligible change thereafter. The ECSA retention of Pt/Nb-SnO₂/VGCF was quite high at 72.0% even after 400,000 load potential cycles, compared with just 14.0% for Pt/C.

Representative TEM images of Pt/Nb-SnO₂/VGCF electrocatalysts before and after 400,000 load potential cycles are shown in Figure 13. The Pt particle diameter of each electrocatalyst derived from the TEM images is shown in Figure 14. For Pt/Nb-SnO₂/VGCF, very little growth in the Pt nanoparticle size is observed, in agreement with the stable ECSA. On the other hand, the Pt nanoparticles in Pt/C dramatically increase in size, explaining the decrease in ECSA and cell voltage after 400,000 load potential cycles.

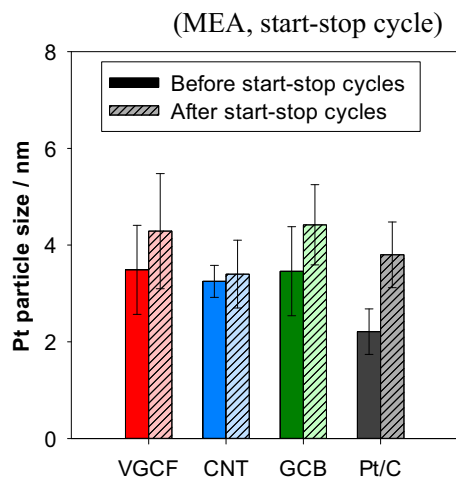


Figure 9. Change in average Pt nanoparticle size in Pt/Nb-SnO₂/VGCF, Pt/Nb-SnO₂/CNT, Pt/Nb-SnO₂/GCB, and Pt/C electrocatalysts, before and after 60,000 start-stop potential cycles.

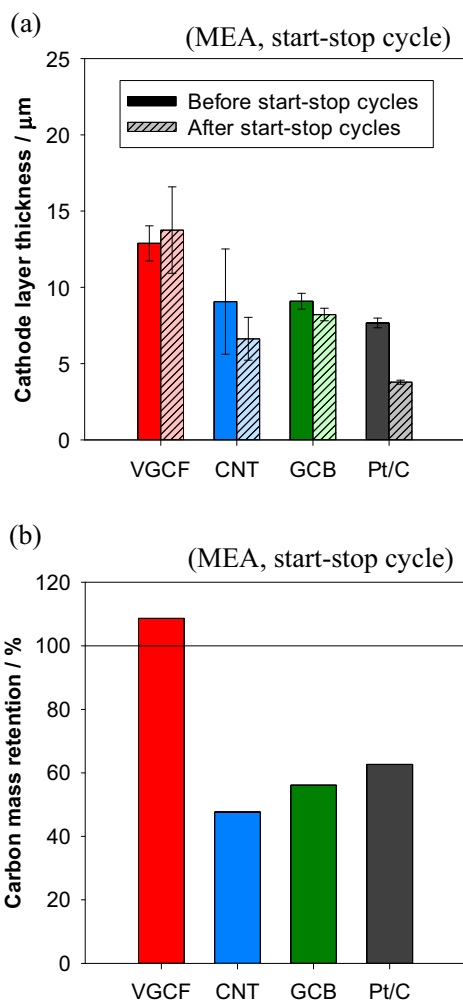


Figure 10. (a) Change in cathode layer thickness and (b) carbon weight retention of MEAs made with Pt/Nb-SnO₂/VGCF, Pt/Nb-SnO₂/CNT, Pt/Nb-SnO₂/GCB, and Pt/C, after 60,000 start-stop potential cycles.

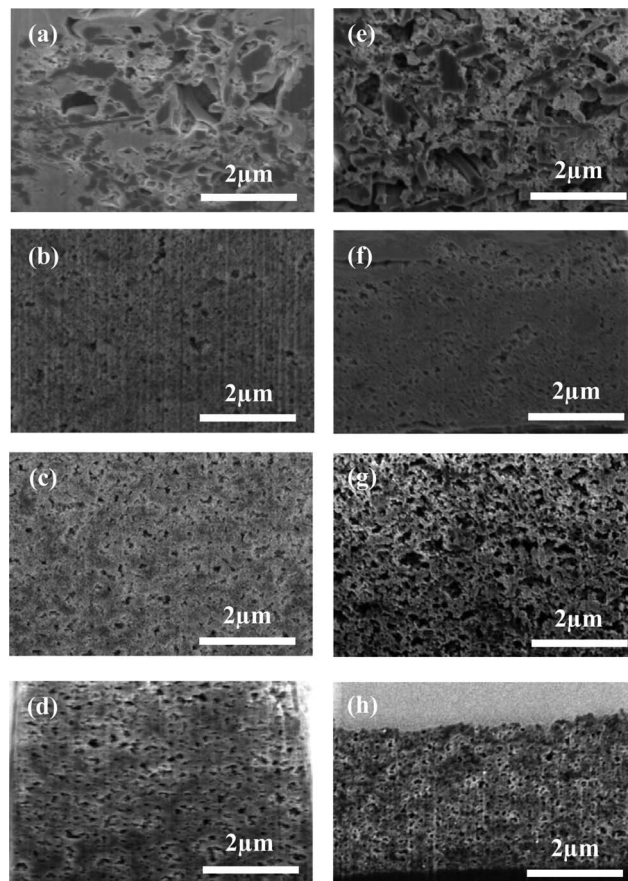


Figure 11. FIB-SEM images of MEA cathode cross-sections (a-d) before and (e-h) after 60,000 start-stop potential cycles: (a,e) Pt/Nb-SnO₂/VGCF, (b,f) Pt/Nb-SnO₂/CNT, (c,g) Pt/Nb-SnO₂/GCB, and (d,h) Pt/C.

By using the SnO₂ support, catalyst degradation associated with Pt nanoparticle mobility is likely to be inhibited due to the high binding energy between Pt and SnO₂ compared to that between Pt and carbon.⁴¹ Consequently, the Pt diameter does not change even after 400,000 load potential cycles, leading to stable ECSA in the MEA. However, the cell voltage did decrease. The reasons for this are unclear at present, but we speculate that it may be due to suppression of the electronic conductivity due to oxygen adsorption on SnO₂. It is known from the field of gas sensors that when oxygen is adsorbed onto SnO₂ surfaces it can form a high-resistance electronic depletion layer by withdrawing electrons from the surface.^{53,54} Whilst the deposition of Pt on SnO₂ may inhibit this effect to some extent,⁵⁵ such insulating O₂-adsorbed SnO₂ surfaces, if present, could explain the decreasing cell voltage whilst the ECSA remains constant. Recently, suppression of dissolution associated with Ostwald ripening at high potentials was reported for Pt catalysts supported on Sb-doped SnO₂, by Binninger et al.⁵⁶ This was attributed to possible potential-dependent conductivity changes in the space-charge region near the SnO₂ surface.

Detailed mechanisms of such MEA performance degradation with SnO₂-based catalyst supports in load cycling protocols should be clarified in future studies. Deeper analyses are needed to understand these real-world phenomena and to give further insights into electrocatalyst stability, including: e.g. Pt-oxide support interaction by X-ray photoelectron spectroscopy (XPS) analysis; changes in MEA conductivity before and after voltage cycling by impedance spectroscopy; and fingerprints of elements including Pt before and after voltage cycling. Besides Pt-decorated SnO₂-supported PEFC electrocatalysts discussed in this study, such detailed durability studies on potential cycling are also needed for various oxide-based electrocatalysts⁵⁷⁻⁶¹ including: e.g. oxide-core Pt-shell

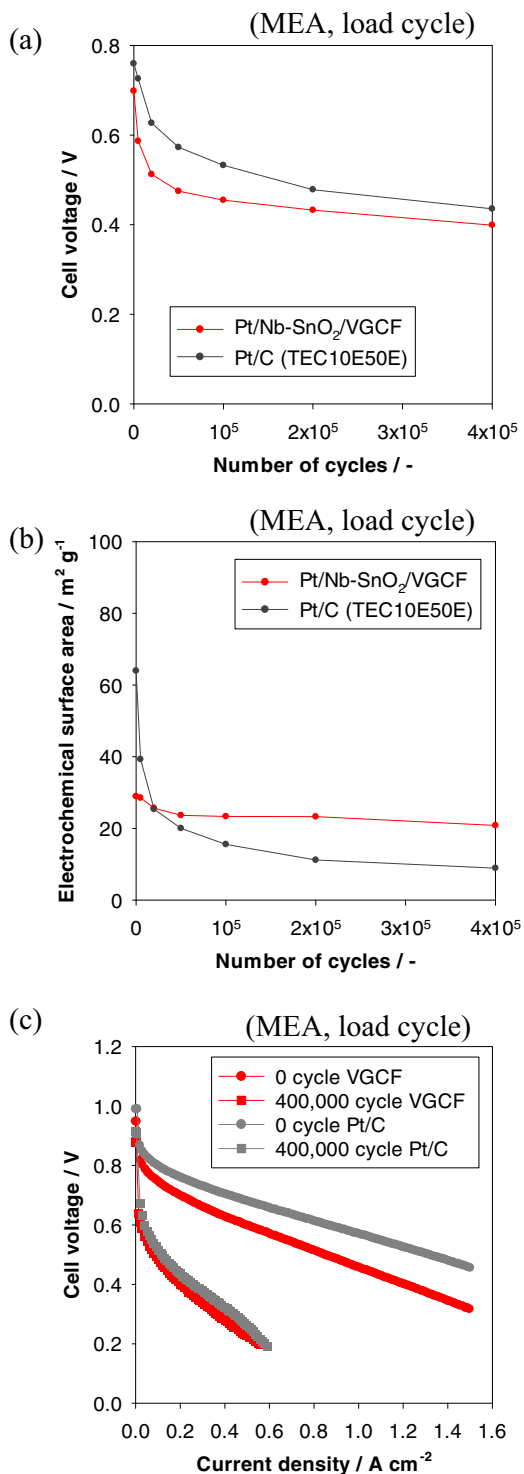


Figure 12. (a) Cell voltage at 0.2 Acm⁻², (b) ECSA, and (c) I-V characteristics before and after 400,000 load potential cycles for Pt/Sn(Nb)O₂/VGCF and conventional Pt/C electrocatalyst layers.

electrocatalysts,⁵⁷ carbon-free all-in-one electrodes using porous Ti sheets,⁵⁸ Pt-decorated oxide/MPL/GDL-supported MEAs,⁵⁹ carbon-free SnO₂-supported electrocatalysts^{22,23,61} for PEFCs, as well as metal-oxide-supported electrocatalysts for polymer electrolyte membrane water electrolysis.⁶⁰ Detailed microstructural analyses should be combined if degradation of such electrocatalyst layers is associated with microstructural/nanostructural changes.⁶²⁻⁶⁵ Further increase in

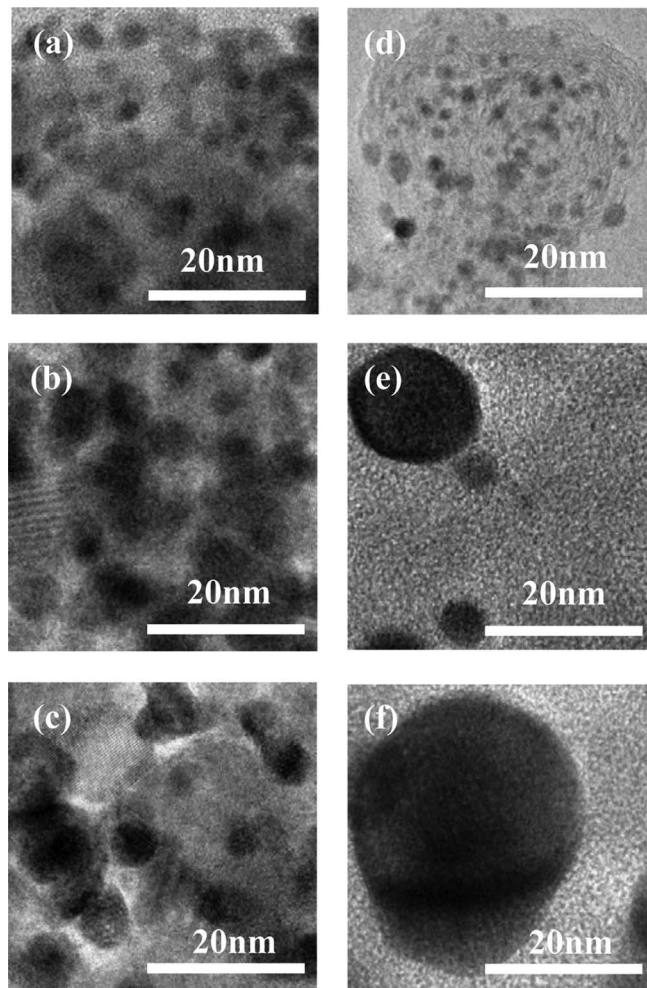


Figure 13. TEM images of Pt/Nb-SnO₂/VGCF electrocatalysts (a) before, and after 400,000 load potential cycles (b) near the electrolyte membrane, and (c) near the carbon paper. TEM images of conventional Pt/C electrocatalysts (d) before, and after 400,000 load potential cycles (e) near the electrolyte membrane, and (f) near the carbon paper are also shown for comparison.

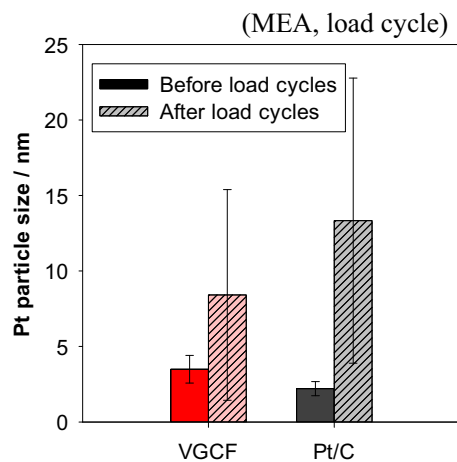


Figure 14. Pt particle size of Pt/Nb-SnO₂/VGCF and conventional Pt/C electrocatalysts, before and after 400,000 load potential cycles.

catalytic activity by alloying Pt with Co and Ni is described in Part II of this study by Matsumoto et al.⁶⁶

Conclusions

Pt-decorated Nb-SnO₂ catalyst supports on three different types of conductive carbon fillers (VGCF, CNT, and GCB) were investigated. Among these, Pt/Nb-SnO₂/CNT exhibited the highest initial electrocatalytic activity. MEAs were fabricated using these different electrocatalysts, and the Nafion content was varied to optimize the microstructure of the electrocatalyst layer, resulting in relatively high I-V performance. The microstructure of the cathode layer using Pt/Nb-SnO₂/VGCF had a wide pore size distribution compared to the relatively dense microstructure of the other electrocatalyst layers. Microstructures with a wider pore size distribution led to better I-V performance, especially in the high current density region. With respect to durability, the Pt/Nb-SnO₂/VGCF MEA exhibited excellent start-stop cycle durability. This MEA also exhibited better durability than the conventional Pt/C over 400,000 load potential cycles. This study indicates that Pt-decorated SnO₂-supported electrocatalysts deposited on conductive fillers can realize high catalytic activity, sufficient electrochemical characteristics, excellent start-stop cycle durability, and sufficient load cycle durability, simultaneously in both half-cell and full-cell MEA conditions. As such, they display great potential for application in highly durable PEFCs in the future.

Acknowledgments

Financial support by the Center-of-Innovation (COI) program, JST Japan, is gratefully acknowledged.

ORCID

K. Sasaki  <https://orcid.org/0000-0002-3174-9087>

References

- J. Larminie and A. Dicks, *Fuel Cell Systems Explained*, 2nd ed., John Wiley & Sons, England (2003).
- W. Viestich, H. A. Gasteiger, and A. Lamm, *Handbook of Fuel Cells: Fundamentals, technology, and application, fuel cell technology and applications*, Vols. 3 & 4. New York: John Wiley & Sons (2003).
- C. A. Reiser, L. Bregoli, T. W. Patterson, J. S. Yi, D. Yang, M. L. Perry, and T. D. Jarvi, *Electrochem. Solid-State Lett.*, **8**(6), A273 (2005).
- L. M. Roen, C. H. Park, and T. D. Jarvi, *Electrochem. Solid-State Lett.*, **7**(1), A19 (2004).
- J. P. Meyers and R. M. Darling, *J. Electrochem. Soc.*, **153**(8), A1432 (2006).
- S. Maass, F. Finsterwalder, G. Frank, R. Hartmann, and C. Merten, *J. Power Sources*, **176**(2), 444 (2008).
- J. Liu, D. Takeshi, K. Sasaki, and S. M. Lyth, *Fuel Cells*, **14**(5), 728 (2014).
- Y. Shao, S. Zhang, C. Wang, Z. Nie, J. Liu, Y. Wang, and Y. Lin, *J. Power Sources*, **195**(15), 4600 (2010).
- Y. Shao, G. Yin, J. Zhang, and Y. Gao, *Electrochim. Acta*, **51**, 5853 (2006).
- S. V. Selvaganesh, P. Sridhar, S. Pitchumani, and A. K. Shukla, *J. Solid-State Electrochem.*, **18**(5), 1291 (2014).
- P. V. Shanahan, L. Xu, C. Liang, M. Waje, S. Dai, and Y. S. Yan, *J. Power Sources*, **185**(1), 423 (2008).
- Y. Minamida, X. Zhao, Z. Noda, A. Hayashi, and K. Sasaki, *ECS Trans.*, **58**(1), 1105 (2013).
- J. Liu, D. Takeshi, K. Sasaki, and S. M. Lyth, *Fuel Cells*, **14**(5), 728 (2014).
- T. Ioroi, H. Senoh, S. Yamazaki, S. Yamazaki, Z. Siroma, N. Fujiwara, and K. Yasuda, *J. Electrochem. Soc.*, **155**(4), B321 (2008).
- K. W. Park and K. S. Seol, *Electrochem. Comm.*, **9**(9), 2256 (2007).
- S. Y. Huang, P. Ganesan, S. Park, and B. N. Popov, *J. Am. Chem. Soc.*, **131**(39), 13898 (2009).
- H. Chhina, S. Campbell, and O. Kesler, *J. Electrochem. Soc.*, **154**(6), B533 (2007).
- M. Pourbaix, *Atlas of Electrochemical Equilibria in Aqueous Solutions*, 2nd ed., National Association of Corrosion Engineers (1974).
- K. Sasaki, F. Takasaki, Z. Noda, S. Hayashi, Y. Shiratori, and K. Ito, *ECS Trans.*, **33**(1), 473 (2010).
- Y. Takabatake, Z. Noda, S. M. Lyth, A. Hayashi, and K. Sasaki, *International J. Hydrogen Energy*, **39**(10), 5074 (2014).
- T. Kuroki, K. Sasaki, H. Kusaba, and Y. Teraoka, 206th ECS meeting abstract, MA2004-02, #1527 (2004).
- A. Masao, S. Noda, F. Takasaki, K. Ito, and K. Sasaki, *Electrochem. Solid-State Lett.*, **12**(9), B119 (2009).
- F. Takasaki, S. Matsue, Y. Takabatake, Z. Noda, A. Hayashi, Y. Shiratori, K. Ito, and K. Sasaki, *J. Electrochem. Soc.*, **158**(10), B1270 (2011).
- K. Kanda, Z. Noda, Y. Nagamatsu, T. Higashi, S. Taniguchi, S. M. Lyth, A. Hayashi, and K. Sasaki, *ECS Electrochem. Lett.*, **3**(4), F15 (2014).
- T. Tsukatsune, Y. Takabatake, Z. Noda, T. Daio, A. Zaitou, S. M. Lyth, A. Hayashi, and K. Sasaki, *J. Electrochem. Soc.*, **161**(12), F1208 (2014).
- G. Ozouf, G. Cognard, F. Maillard, L. Guetaz, M. Heitzmann, and C. Beauger, *ECS Trans.*, **69**(17), 1207 (2015).
- W. S. Baker, J. J. Pietron, M. E. Teliska, P. J. Bouwman, D. E. Ramaker, and K. E. Swider-Lyons, *J. Electrochem. Soc.*, **153**(9), A1702 (2006).
- T. Tada, Y. Yamamoto, K. Matsutani, K. Hayakawa, and T. Namai, *ECS Trans.*, **16**(2), 215 (2008).
- M. Nakada, A. Ishihara, S. Mitsushima, N. Kamiya, and K. Ota, *Electrochem. Solid-State Lett.*, **10**(1), F1 (2007).
- K.-S. Lee, I.-S. Park, Y.-H. Cho, D.-S. Jung, N. Jung, H.-Y. Park, and Y.-E. Sung, *J. Catal.*, **258**(1), 143 (2008).
- K. Kakinuma, M. Uchida, T. Kamino, H. Uchida, and M. Watanabe, *Electrochem. Acta*, **56**(7), 2881 (2011).
- P. K. Mohana, C. Glöckler, A. O. Arenas, and L. Jonssen, *International J. Hydrogen Energy*, **42**(46), 27950 (2017).
- W. Q. Han and A. Zettl, *Nano Lett.*, **3**(5), 681 (2003).
- D. Horiguchi, Z. Noda, A. Hayashi, and K. Sasaki, 228th ECS meeting abstract, MA2015-02, 1394 (2015).
- X. Li, J. Wei, Y. Chai, and S. Zhang, *J. Colloid Interface Sci.*, **450**, 74 (2015).
- Y. Nakazato, D. Kawachino, Z. Noda, J. Matsuda, A. Hayashi, and K. Sasaki, *ECS Trans.*, **80**(8), 897 (2017).
- K. Matsumoto, T. Fujigaya, K. Sasaki, and N. Nakashima, *J. Mater. Chem.*, **21**(4), 1187 (2011).
- M. R. Berber, T. Fujigaya, K. Sasaki, and N. Nakashima, *Sci. Rep.*, **3**, 1764 (2013).
- K. Sasaki, K. Shinya, S. Tanaka, Y. Kawazoe, T. Kuroki, K. Tanaka, H. Kusaba, and Y. Teraoka, *Mater. Res Soc. Symp. Proc.*, **835**, 241 (2005).
- X. Zhao, A. Hayashi, Z. Noda, K. Kijima, I. Yagi, and K. Sasaki, *Electrochim. Acta*, **97**, 33 (2013).
- T. Daio, A. Staykov, L. Guo, M. Tanaka, S. M. Lyth, and K. Sasaki, *Sci. Rep.*, **5**, 13126 (2015).
- A. Hayashi, H. Notsu, K. Kimizima, J. Miyamoto, and I. Yagi, *Electrochim. Acta*, **53**, 6117 (2008).
- A. Ohma, K. Shinohara, A. Iiyama, T. Yoshida, and A. Daimaru, *ECS Trans.*, **41**(1), 775 (2011).
- M. Hori, K. Kobayashi, Y. Oono, and A. Daimaru, 222nd ECS meeting abstract, MA2012-02, 1497 (2012).
- New Energy and Industrial Technology Development Organization (NEDO), <http://www.nedo.go.jp/content/100537904.pdf> (accessed 2017-12-6).
- R. Yadav and P. S. Fedkiw, *J. Electrochem. Soc.*, **159**(3), B340 (2012).
- Y. Sone, P. Ekduunge, and D. Simonsson, *J. Electrochem. Soc.*, **143**(4), 1254 (1996).
- S. C. Tsang, Y. K. Chen, P. J. F. Harris, and M. L. H. Green, *Nature*, **372**, 159 (1994).
- K. Balasubramanian and M. Burghard, *Small*, **1**(2), 180 (2005).
- T. Fujigaya and N. Nakashima, *Polymer Journal*, **40**(7), 577 (2008).
- M. Okumura, Z. Noda, J. Matsuda, Y. Tachikawa, M. Nishihara, S. M. Lyth, A. Hayashi, and K. Sasaki, *J. Electrochem. Soc.*, **164**(9), F928 (2017).
- M. Lee, M. Uchida, H. Yano, D. A. Tryk, H. Uchida, and M. Watanabe, *Electrochim. Acta*, **55**, 8504 (2010).
- J. Maier, *Physical Chemistry of Ionic Materials Ions and Electrons in Solids*, John Wiley & Sons, (2004).
- M. Batzill and U. Diebold, *Progress in Surface Science*, **79**(2-4), 47 (2005).
- Y. Senoo, K. Kakinuma, M. Uchida, H. Uchida, S. Deki, and M. Watanabe, *RSC Adv.*, **4**(61), 32180 (2014).
- T. Binninger, R. Mohamed, A. Patru, K. Waltar, E. Gericke, X. Tuavev, E. Fabbri, P. Leveque, A. Hoell, and T. J. Schmidt, *Chem. Mater.*, **29**(7), 2831 (2017).
- M. Nagamine, Z. Noda, H. Manabe, J. Matsuda, A. Hayashi, and K. Sasaki, *ECS Trans.*, **86**(13), 531 (2018).
- D. Kawachino, M. Yasutake, H. Odoi, Z. Noda, J. Matsuda, A. Hayashi, and K. Sasaki, *ECS Trans.*, **86**(13), 541 (2018).
- H. Odoi, Z. Noda, J. Matsuda, A. Hayashi, and K. Sasaki, *ECS Trans.*, **86**(13), 461 (2018).
- M. Yasutake, H. Anai, D. Kawachino, Z. Noda, J. Matsuda, K. Ito, A. Hayashi, and K. Sasaki, *ECS Trans.*, **86**(13) 673 (2018).
- K. Kakinuma, R. Kobayashi, A. Iiyama, and M. Uchida, *J. Electrochem. Soc.*, **165**(15), J3083 (2018).
- D. A. Cullen, R. Koestner, R. S. Kukreja, Z. Y. Liu, S. Minko, O. Trotsenko, A. Tokarev, L. Guetaz, H. M. Meyer III, C. M. Parish, and K. L. More, *J. Electrochem. Soc.*, **161**, F1111 (2014).
- L. Guetaz, M. Looez-Haro, S. Escibano, A. Morin, G. Gebel, D. Cullen, K. More, and R. Borup, *ECS Trans.*, **69**(17), 455 (2015).
- G. Inoue and M. Kawase, *J. Power Sources*, **327**, 1 (2016).
- H. Manabe, Y. Nakazato, M. Okumura, J. Matsuda, Z. Noda, A. Hayashi, and K. Sasaki, *ECS Trans.*, **86**(13), 69 (2018).
- S. Matsumoto, M. Nagamine, Z. Noda, J. Matsuda, S. M. Lyth, A. Hayashi, and K. Sasaki, *J. Electrochem. Soc.*, **165**, 1164 (2018).